Textural Mesoporosity and the Catalytic Activity of Mesoporous Molecular Sieves with Wormhole Framework Structures

Thomas R. Pauly,[†] Yu Liu,[†] Thomas J. Pinnavaia,*[,†] Simon J. L. Billinge,[‡] and Thomas P. Rieker[§]

Contribution from the Department of Chemistry and Center for Fundamental Materials Research, Department of Physics and Astronomy, Michigan State University, East Lansing, Michigan 48824, and Center for Microengineered Materials and Department of Chemical and Nuclear Engineering, University of New Mexico, Albuquerque, New Mexico 87131

Received April 28, 1999

Abstract: Three different water−alcohol cosolvent systems were used to assemble mesoporous molecular sieve silicas with wormhole framework structures (previously denoted HMS silicas) from an electrically neutral amine surfactant (S°) and a silicon alkoxide precursor (I°). The fundamental particle size and associated textural (interparticle) porosity of the disordered structures were correlated with the solubility of the surfactant in the water−alcohol cosolvents used for the S°I° assembly process. Polar cosolvents containing relatively low volume fractions of $C_nH_{2n+1}OH$ alcohols ($n = 1-3$) gave heterogeneous surfactant emulsions that assembled intergrown aggregates of small primary particles with high textural pore volumes (designated HMS−HTx). Conversely, three-dimensional, monolithic particles with little or no textural porosity (designated HMS−LTx) were formed from homogeneous surfactant solutions in lower polarity cosolvents. Aluminum substituted Al-HMS−HTx analogues with high textural porosity and improved framework accessibility also were shown to be much more efficient catalysts than Al-HMS−LTx or monolithic forms of hexagonal Al-MCM-41 for the sterically demanding condensed phase alkylation of 2,4-di-*tert*-butylphenol with cinnamyl alcohol. Transmission electron microscopy (TEM) and small-angle X-ray scattering (SAXS) studies verified the textural differences between wormhole HMS and electrostatically assembled hexagonal MCM-41 and SBA-3 molecular sieves. Power law fits to the scattering data indicated a surface fractal ($D_s = 2.76$) for HMS−HTx, consistent with rough surfaces. A second power law at lower-q indicated the formation of a mass fractal ($D_m = 1.83$) consistent with branching of small fundamental particles. Hexagonal MCM-41 and SBA-3 silicas, on the other hand, exhibited scattering properties consistent with moderately rough surfaces ($D_s = 2.35$ and 2.22, respectively) and large particle diameters ($\gg 1\ \mu$m). HMS−LTx silicas showed little or no mass fractal character ($D_m = 2.87$), and no surface fractal scattering.

Introduction

Several general pathways have been developed in recent years for the assembly of mesoporous molecular sieves. These pathways may be classified according to electrostatic charge matching,[1,2,3] hydrogen bonding,[4,5] and dative bonding[6] interactions at the interface of the structure-directing surfactant micelles and the inorganic framework. The benefits of electrically neutral amine surfactants for the H-bonded assembly of mesostructures have been demonstrated by the properties of silica molecular sieves assembled in the presence of amine surfactants.[7,8] Originally described as disordered hexagonal molecular silicas and denoted HMS, these latter neutral framework silicas have more recently been shown to possess wormhole-like or spongelike framework structures[4,8] rather than the long-range hexagonal framework structures characteristic of electrostatically assembled MCM-41 and SBA-3 silicas.[1,3] Nevertheless, the pore-size distributions, surface areas, and pore volumes of HMS silicas are similar to those of electrostatically assembled mesostructures. The wormhole channel motif is a potentially important structural feature for favorable catalytic reactivity, in part, because channel branching within the framework can facilitate access to reactive sites on the framework walls. HMS wormhole structures can also have relatively small fundamental particle sizes (<200 nm), which result in complementary textural mesoporosity for the more efficient transport of reagents to framework reaction centers.[8] This catalytically important textural porosity arises from the aggregation of small fundamental

[†] Department of Chemistry and Center for Fundamental Materials Research, Michigan State University.

[‡] Department of Physics and Astronomy, Michigan State University.

[§] Center for Microengineered Materials and Department of Chemical and Nuclear Engineering, University of New Mexico.

(1) Beck, J. S.; Vartuli, J. C.; Roth, W. J.; Leonowicz, M. E.; Kresge, C. T.; Schmitt, K. D.; Chu, C. T−W.; Olson, D. H.; Sheppard, E. W.; McCullen, B.; Higgins, J. B.; Schlenker, J. L. *J. Am. Chem. Soc.* **1992**, *114*, 10834.

(2) Huo, Q.; Margolese, D. I.; Ciesla, U.; Demuth, D. G.; Feng, P.; Gier, T. E.; Sieger, P.; Firouzi, A.; Chmelka, B. F.; Schüth, F.; Stucky, G. D. *Chem. Mater.* **1994**, *6*, 1176.

(3) Huo, Q.; Margolese, D. I.; Ciesla, U.; Feng, P.; Gier, T. E.; Sieger, P.; Leon, R.; Petroff, P. M.; Schüth, F.; Stucky, G. D. *Nature* **1994**, *368*, 317.

(4) Tanev, P. T., and Pinnavaia, T. J. *Science* **1995**, *267*, 865.

(5) Bagshaw, S. A.; Prouzet, E.; Pinnavaia, T. J. *Science* **1995**, 269, 1242; Bagshaw, S. A.; Pinnavaia, T. J. *Angew. Chem., Int. Ed. Engl.* **1996**, *35*, 1102.; Prouzet, E.; Pinnavaia, T. J. *Angew. Chem., Int. Ed. Engl.* **1997,** *36*, 516.

(6) Antonelli, D. M.; Ying, J. Y. *Angew. Chem., Int. Ed. Engl.* **1996**, *35*, 426; Antonelli, D. M.; Ying, J. Y. *Chem. Mater.* **1996**, *8*, 874.

(7) Tanev, P.T.; Pinnavaia, T. J. *Chem. Mater.* **1996**, *8*, 2068.

(8) Zhang, W.; Pauly, T. R.; Pinnavaia, T. J. *Chem. Mater.* **1997**, *9*, 2491.

10.1021/ja991400t CCC: $18.00
Published on Web 09/10/1999

particles through intergrowth or other associative mechanisms. Consequently, textural porosity is dependent on the size, connectivity, and surface texture of the fundamental particles, but it is independent of the framework structure of the particles.

The textural mesoporosity of HMS silicas is determined by the polarity of the medium in which the framework is assembled. Highly polar solvents, such as 90:10 (v:v) water−ethanol, characteristically afford wormhole frameworks with fundamental particle sizes < 200 nm and textural mesopores that are comparable to the framework pores in overall volume.[8] However, solvents of relatively low polarity, e.g., 35:65 (v:v) water−ethanol, promote the growth of large, monolithic particles with little or no textural porosity.

The importance of textural mesopores in enhancing the catalytic activity of HMS materials relative to MCM-41 has been demonstrated for several condensed phase reactions in which access to framework reaction sites may be diffusion limited. Substantially higher conversions have been reported for the peroxide oxidation of various substrates using Ti-,[9−11] V-,[11−14] Cr-,[11] Mo-,[11] and Mn-[11]substituted HMS materials compared to analogous compositions of MCM-41. Also, Fe^{3+} exchanged Al-HMS exhibits a higher rate constant for the selective catalytic reduction of NO by NH_3 than does Fe^{3+} exchanged Al-MCM-41.[15] Additionally, Al-HMS is more active for the cracking of cumene[16] than a compositionally equivalent Al-MCM-41. On the other hand, Ti-HMS has been reported to exhibit *lower* catalytic activity than Ti-MCM-41 for the peroxide epoxidation of α-pinene[17] and the oxidation of aniline.[18]

The discrepancies in assessing the relative catalytic activities of HMS and MCM-41 materials may be linked to differences in textural properties. Although the Ti-HMS used for aniline oxidation was prepared at solvent composition that should have provided a product with high textural porosity, the N_2 adsorption[19] properties indicated the *absence* of textural pores. This latter result suggested to us that the textural mesoporosity of HMS materials might be much more sensitive to solvent polarity than previously realized. Accordingly, the present work investigates the textural mesoporosity of HMS molecular sieve silicas assembled from cosolvent mixtures of water and three different $C_nH_{2n+1}OH$ alcohols ($n = 1-3$). Representative Al-substituted HMS derivatives with relatively high and low textural mesoporosity, designated Al-HMS−HTx and Al-HMS−LTx, respectively, are compared as catalysts, along with Al-MCM-41, for the catalytic alkylation of 2,4-di -*tert*-butylphenol with cinnamyl alcohol. This sterically demanding condensed phase reaction provides a clear assessment of the role of textural mesoporosity in determining the relative catalytic activities of mesoporous molecular sieves with equivalent framework pore sizes. In addition, SAXS and TEM studies have been used to characterize the textural properties of wormhole HMS materials. Representative hexagonal mesostructures, namely, MCM-41[20,21] and SBA-3,[3] as prepared by previously reported electrostatic assembly pathways, have been included in the SAXS studies for comparison.

Experimental Section

Syntheses. Solvents of differing polarity for HMS syntheses were prepared by combining different volumes of H_2O and a less polar alcohol cosolvent. A typical reaction series used methanol, ethanol, or propanol as a cosolvent and dodecylamine (abbreviated DDA) as the structure directing surfactant, S°. The synthesis of a HMS molecular sieves with relatively high or low textural mesoporosity was carried out by first dissolving 1.2 g DDA (6.47 mmol) into the desired volume of alcohol and the diluting the solution to a total volume of 28 mL with water. A 5-g portion (24.0 mmol) of the I° precursor, tetraethyl orthosilicate (TEOS), was then added to the surfactant solution under vigorous stirring. The reaction solution was stirred at ambient temperature for 20 h in a sealed flask.

Aluminum-substituted HMS analogues with high and low textural mesoporosities were obtained by first preparing the pure silica mesostructures according to the above procedure in water: ethanol mixtures at volume ratios of 60:40 and 50:50, respectively. After a reaction time of 20 h, a solution of $Al(OCH(CH_3)CH_2CH_3)_3$ in 5 mL of *sec*-butanol and 5 mL of ethanol was added to the HMS reaction mixtures. The reaction mixtures were subsequently heated at 45 °C for an additional 20 h. The as-synthesized HMS and Al-HMS reaction products were filtered, washed with H_2O and air-dried at ambient temperature for 24 h. Surfactant removal from each product was accomplished by calcination at 630 °C for 4 h in air. The calcination temperature was reached using a ramping rate of 2 °C/min.

Hexagonal SBA-3[3] and MCM-41[20,21] molecular sieve silicas were prepared by electrostatic assembly pathways according to previously reported methods. $C_{16}H_{33}N(CH_3)_3Br$ (CTAB) was the surfactant used in the synthesis of both materials in order to obtain framework pore sizes comparable to the HMS silicas used in this study. Aluminum-substituted MCM-41 was prepared by adding $Al(NO_3)_3$ to the MCM-41 reaction mixture after 24 h reaction at 100 °C,[22] and then continuing the reaction for an additional 24 h at 100 °C.

Catalytic Reactions. The alkylation of 2,4-di-*tert*-butylphenol with cinnamyl alcohol was carried out in a 100-mL flask with 1.0 mmol 2,4-di-*tert*-butylphenol (Aldrich) and 1.0 mmol cinnamyl alcohol (Aldrich) using 50.0 mL isooctane as a solvent. The solution was heated to 60 °C and 500 mg catalyst was added. After a reaction time of 6 h, the catalyst was filtered and extracted with dichloromethane to recover adsorbed reaction products. The solutions from the reaction and the catalyst extraction were combined and distilled to remove the solvent. The products were analyzed by GC (HP 5890) and GC−MS using 1,3 di-*tert*-butylbenzene as an internal standard.

Physical Measurements. Wide-angle powder X-ray diffraction (XRD) patterns were obtained using a Rigaku Rotaflex Diffractometer with Cu Kα radiation ($\lambda = 0.154$ nm). Counts were accumulated every 0.02° (2θ) at a scan speed of 1° (2θ)/min. Shifts in the position of the first correlation peak for HMS samples were taken as being indicative of changes in the average pore−pore separation.

N_2 adsorption−desorption isotherms were obtained at −196 °C on a Micromeritics ASAP 2010 Sorptometer using static adsorption procedures. Samples were outgassed at 150 °C and 10^{-6} Torr for a minimum of 12 h prior to analysis. BET surface areas were calculated from the linear part of the BET plot according to IUPAC[23] recommendations. Pore-size distribution was estimated from the adsorption branch of the isotherm by the method of Horvath and Kawazoe.[24] The

(9) Tanev, P. T., Chibwe, M., and Pinnavaia, T. J. *Nature* **1994**, 368, 321.
(10) Zhang, W.; Fröba, M.; Wang, J.; Tanev, P. T.; Pinnavaia, T. J. *J. Am. Chem. Soc*. **1996**, *118*, 9164.
(11) Zhang, W.; Wang, J.; Tanev, P. T.; Pinnavaia, T. J. *J. Chem. Soc., Chem. Commun*. **1996**, 253.
(12) Reddy, J. S.; Moudrakovski, I.; Sayari, A. *J. Chem. Soc., Chem. Commun*. **1994**, 1059.
(13) Reddy, J. S.; Sayari, A. *J. Chem. Soc., Chem. Commun*. **1995**, 2231.
(14) Reddy, J. S.; Lui, P.; I.; Sayari, A. *Appl. Catal. A* **1996**, *7*, 148.; Sayari, A. *Chem. Mater*. **1996**, *8*, 1840.
(15) Yang, R.; Pinnavaia, T. J.; Li, W.; Zhang, W. *J. Catal*. **1997**, *172*, 488.
(16) Kloetstra, K. R.; van Bekkum, H.; Jansen, J. C. *J. Chem. Soc., Chem. Commun*. **1997**, 2281.
(17) On, T. D.; Kapoor, M. P.; Joshi, P. N.; Bonneviot, L.; Kaliaguine, S. *Catal. Lett*. **1997**, *44*, 171.
(18) Gontier, S.; Tuel, A. *J. Catal*. **1995**, 157, 124.
(19) Gontier, S.; Tuel, A. *Chem. Mater*. **1996**, *8*, 114.
(20) Edler, K. J.; Dougherty, J.; Durand, R.; Iton, L.; Kirton, G.; Lockhart, G.; Wang, Z.; Withers, R.; White, J. W. *Colloids Surf. A* **1995**, *102*, 213.
(21) Edler, K. J.; White, J. W. *Chem. Mater*. **1997**, *9*, 1226.
(22) Zhang, W.; Liu, Y.; Pinnavaia, T. J., manuscript in preparation.
(23) Sing, K. S. W.; Everett, D. H.; Haul, R. A. W.; Moscou, L.; Pierrotti, R. A.; Rouquerol, J.; Siemieniewska, T. *Pure Appl. Chem*. **1985**, *57*, 603.
(24) Horvath, G.; Kawazoe, K. J. *J. Chem. Eng. Jpn*. **1983**, *16*, 470.

framework pore volume (V_f) for each mesostructured sample is taken as the volume adsorbed at 0.50 P/P_0, whereas the total pore volume (V_t) is the volume adsorbed at 0.99 P/P_0. Textural pore volume (V_{tx}) is the difference ($V_t - V_f$).

TEM images were obtained on a JEOL 100CX microscope with a CeB_6 filament and an accelerating voltage of 120 KV. Samples were prepared by sonicating the powdered sample for 20 min in EtOH and then evaporating two drops onto carbon-coated copper grids.

SAXS experiments were conducted at the University of New Mexico/Sandia National Laboratories Small-angle X-ray Scattering Laboratory (http://saxs-comm.unm.edu). Samples approximately 0.07−0.27 mm thick were prepared by sprinkling the powdered samples on adhesive cellophane tape used as windows on a 1.5-cm inner diameter washer. Data were collected and combined for the samples and backgrounds on the Bonse−Hart ($0.0003 < q < 0.1$ Å^{-1}) and 5-m pinhole ($0.03 < q < 0.7$ Å^{-1})[25] instruments using Cu Kα radiation. The wave vector q is defined as, $q = 4\pi/\lambda \sin(2\theta/2)$, where 2θ is the scattering angle. Scattering data from the two instruments is corrected for background, slit smearing, and sample thickness before being combined.

Results and Discussion

Mesostructure Synthesis. In order to better elucidate the relationship between the textural porosity of wormhole HMS molecular sieves and the polarity of the solvent system from which they are assembled, a series of samples were prepared in three different $H_2O-C_nH_{2n+1}OH$ ($n = 1$, 2, and 3) cosolvents. For each reaction mixture, dodecylamine was the structure-directing surfactant, the surfactant-to-tetraethylorthosilicate ratio (S°/I°) was 0.27, and the concentration of the surfactant was 0.23 M. Clear, homogeneous solutions of the structure-directing surfactant were obtained when the alcohol content by volume was ≥70% methanol, >50% ethanol, and ≥50% propanol. At cosolvent compositions containing lower alcohol concentrations the surfactant formed an emulsion. Thus, at alcohol contents sufficiently high to avoid emulsion formation, the HMS products were nucleated from homogeneous solutions of the surfactant. For cosolvents with lower alcohol concentrations, the products were assembled from heterogeneous mixtures containing the surfactant in emulsion form.

Aluminum-substituted derivatives of HMS for use in catalytic studies (see below) also were prepared from homogeneous and heterogeneous forms of the surfactant, depending on the choice of the cosolvent composition. The pure silica form of the wormhole mesostructure was formed from either a homogeneous solution (50:50 water:ethanol) or from a heterogeneous surfactant emulsion (60:40 water:ethanol), and then adding sufficient aluminum *sec*-butoxide to the reaction mixture to achieve 2 mol % aluminum incorporation in the framework. This post-assembly procedure for aluminum incorporation made it possible to retain both the wormhole framework structure and the textural properties characteristic of the HMS silica formed from homogeneous and heterogeneous forms of the surfactant. The ^{27}Al MAS NMR spectra of the calcined forms of these Al-HMS derivatives exhibited a single resonance at 64.3 ppm, indicating that all of the aluminum occupied tetrahedral sites in the wormhole framework

Figure 1, A and B are representative X-ray powder diffraction patterns for HMS silicas assembled from heterogeneous emulsion and homogeneous solution forms of the surfactant in cosolvents containing 40 and 50% ethanol by volume, respectively. The XRD patterns for the products obtained from the two forms of the surfactant are indistinguishable. Both products exhibit an intense reflection at low angle and a broad shoulder near 5°. These patterns are typical of HMS wormhole structures assembled from long alkyl chain neutral amines as surfactants, the correlation peak indicating the average pore−pore separation in the disordered wormhole framework. Equivalent XRD patterns were obtained for HMS silicas assembled from water:alcohol cosolvents containing methanol and propanol, regardless of the homogeneity of the initial surfactant solution. The same XRD features also were obtained for the Al-HMS derivatives prepared from heterogeneous and homogeneous forms of the surfactant.

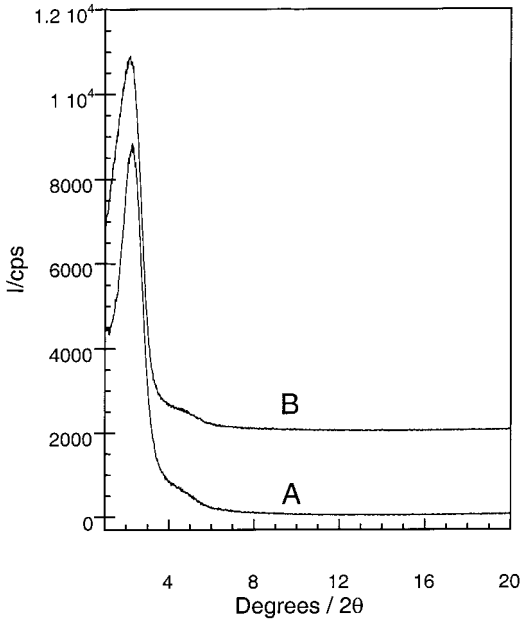

Figure 1. Powder X-ray diffraction patterns of calcined HMS silicas assembled from (A) heterogeneous emulsion and (B) homogeneous solution forms of a dodecylamine surfactant in cosolvents containing 40 and 50% ethanol by volume, respectively. Each sample was prepared at ambient temperature from reaction mixtures containing 0.23 mole/L of dodecylamine and a surfactant/TEOS (S°/I°) ratio of 0.27. As is explained later in the text, sample (A) has a high textural mesoporosity (denoted HMS−HTx) and sample (B) has a relatively low textural mesoporosity (denoted HMS−LTx), but the XRD patterns are indistinguishable. Samples are offset 2000 (cps) for clarity.

Although the HMS molecular sieves formed from a heterogeneous surfactant emulsion or from a homogeneous surfactant solution cannot be distinguished by XRD, the N_2 adsorption properties of the products obtained from these fundamentally different forms of the surfactant differ dramatically. Figure 2, A and B are representative N_2 adsorption−desorption isotherms for HMS silicas prepared from a surfactant emulsion and a surfactant solution, wherein the ethanol content of the cosolvent was 40% and 50 vol %, respectively. Filling of the framework confined mesopores occurs in the partial pressure range 0.15−0.30 for both samples, but only the product formed from the heterogeneous surfactant emulsion shows an additional capillary condensation at partial pressures >0.90 due to the filling of textural mesopores.[7,8] This characteristic signature of textural mesoporosity is observed for *all* HMS materials assembled from heterogeneous emulsions of the amine surfactant in water:alcohol cosolvents, including cosolvents containing methanol and propanol. In contrast, the HMS products obtained from homogeneous solutions of the surfactant showed little or no hysteresis behavior in the textural mesopore region.

Table 1 provides the total pore volume (V_t), framework pore volume (V_f), and textural pore volume (V_{tx}), along with the framework pore diameter and BET surface area, for HMS

(25) Rieker, T. P.; Hubbard, P. F. *Rev. Sci. Instrum.* **1998**, *69*, 3504−3509.

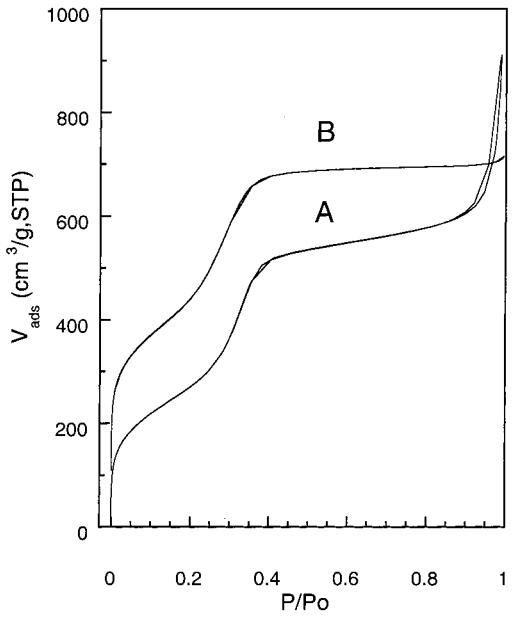

Figure 2. N_2 adsorption−desorption isotherms for calcined HMS silicas assembled from heterogeneous emulsion and homogeneous solution forms of a dodecylamine surfactant in cosolvents containing 40 and 50% ethanol by volume, respectively. Sample A has high textural mesoporosity (HMS−HTx) as indicated by the hysteresis loop at partial pressures >0.90, whereas sample B has low textural mesoporosity (HMS−LTx). The isotherms are offset vertically by 100 cm^3/g, STP for clarity.

derivatives assembled from different water:alcohol cosolvent compositions. The table includes for comparison the analogous values for a hexagonal Al-MCM-41 with a comparable framework pore size. For all of the HMS products assembled from homogeneous surfactant solutions, namely, in cosolvents containing ≥70% methanol, ≥50% ethanol, and ≥50% propanol, the total pore volume is expressed almost entirely as framework porosity and little or no textural porosity (<5% as V_{tx}). These HMS derivatives with low textural porosity, which we denote HMS−LTx, resemble electrostatically assembled MCM-41 in their pore-volume distributions. However, for the mesostructures assembled from surfactant emulsions, at least 20%, and more typically 40−60%, of the total pore volume arises from textural mesopores. Significantly, neither the framework pore volume nor the framework pore size is compromised in these high textural pore derivatives. In fact, the framework pore size, as well as the textural porosity generally increases with decreasing alcohol content of the cosolvent. We denote these high textural porosity materials HMS−HTx.

We consider next the potential importance of textural mesoporosity on the catalytic properties of HMS molecular sieves.

Catalysis Studies. Al-MCM-41 recently has been shown to be an effective solid acid catalyst for the alkylation of 2,4-di-*tert*-butylphenol by cinnamyl alcohol to yield a flavan:[26]

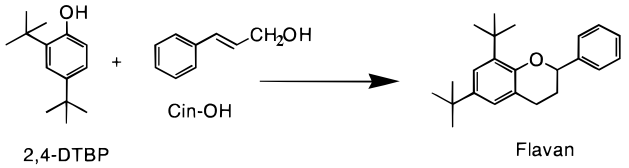

We selected this reaction for evaluating the catalytic significance of textural mesoporosity in HMS mesostructures, in part, because it is a sterically demanding condensed phase transformation and potentially susceptible to diffusion limitations arising from restricted access to the active acid sites in the framework. Also, cinnamyl alcohol self-degrades to unwanted side products, such as the corresponding symmetric ether,[27] under strong acid catalytic conditions. Consequently, the selectivity to flavan is an indicator of the effectiveness of the desired reagent pairing and conversion at the moderately acidic sites within the framework mesopores.

The catalytic properties of Al-HMS−LTx and Al-HMS−HTx, along with those of Al-MCM-41 for comparison are summarized in Table 2. These mesostructures have nearly the same framework pore volume (0.80−0.85 cm^3/g) and the same framework aluminum content (2.0 mol %), as indicated by the data presented in Table 1. They also have the same average framework pore size (3.3−3.4 nm), although the pore distribution is somewhat broader for the Al-HMS derivatives than for Al-MCM-41 (see Figure 3). The incorporation of aluminum into the framework of HMS−HTx reduces the textural pore somewhat, perhaps due to Ostwald ripening at the elevated temperatures used to achieve alumination (cf., Experimental Section). Nevertheless, the textural pore volume is almost four times larger for Al-HMS−HTx than for Al-HMS−LTx and Al-MCM-41. The conversion of cinnamyl alcohol in all cases is 100%, but the conversion of phenol is considerably lower.

Al-HMS−LTx affords the desired flavan in 47.2% yield, comparable to the yield obtained with Al-MCM-41 (49.1%). On the other hand, Al-HMS−HTx provides a flavan yield (56.5%) that is 1.20 times as large as the yield obtained with Al-HMS−LTx and 1.15 times larger than the yield obtained with Al-MCM-41. Factors other than textural mesoporosity may contribute to the differences in the catalytic efficiencies of HMS and MCM-41 mesostructures. These two types of structures (wormhole vs hexagonal frameworks) are assembled by fundamentally different mechanisms (H bonding vs electrostatic assembly). Consequently, the acidic centers may differ in intrinsic strength and accessibility, even though the framework walls are amorphous for both structure types. However, the substantially greater catalytic activity for Al-HMS−HTx compared to Al-HMS−LTx can only be attributed to the four- fold larger textural pore volume, which is important in providing reagent transport to the framework active sites.

TEM and SAXS Studies. TEM images of HMS−HTx and HMS−LTx silicas, prepared from 40 and 50% ethanol cosolvents, respectively, illustrate the differences in the particles sizes and morphologies for these two classes of HMS mesostructures (see Figure 4). Analogous images are observed for all HMS derivatives with high and low textural mesoporosities, regardless of the water: alcohol cosolvent system used for the S°I° assembly process. A HMS−HTx derivative consists of intergrown fundamental particles with a rough, uneven surface (Figure 4A). The intergrowth of small primary particles results in aggregates with significant extraframework void space consistent with the textural mesoporosity observed in N_2 adsorption (Table 2A). Conversely, the HMS−LTx silicas (Figure 4C) obtained from cosolvents of lower polarity have fundamental particle sizes of ∼250 nm or larger. These large, monolithic particles have smoother surfaces and an Euclidean or three-dimensional geometry. However, all HMS−HTx and -LTx derivatives, have disordered wormhole − like frameworks,

(26) Armengol, E.; Cano, M. L.; Corma, A.; Garcia, H.; Navarro, M. T. *J. Chem. Soc., Chem. Commun.* **1995**, 519.

(27) Algarra, F.; Corma, A.; García, H.; Primo, J. *Appl. Catal. A* **1995**, *122*, 125.

Table 1. Textural Properties of Calcined HMS Molecular Sieves Assembled in Water−Alcohol Co-solvents and Calcined Al-MCM-41[a]

sample	cosolvent	vol % alcohol cosolvent	V_t[b] (cc/g)	V_f[c] (cc/g)	V_{tx}[d] (cc/g)	V_{tx}/V_f	pore diameter HK (nm)	BET SA (m^2/g)
HMS−HTx	CH_3OH	40	1.72	0.82	0.90	1.10	3.25	1061
HMS−HTx	CH_3OH	50	1.81	0.73	1.08	1.48	3.01	1041
HMS−HTx	CH_3OH	60	1.20	0.76	0.44	0.58	2.82	1005
HMS−LTx	CH_3OH	70	0.59	0.57	0.02	0.04	2.31	1106
HMS−HTx	C_2H_5OH	30	1.67	0.73	0.94	1.29	2.83	1054
HMS−HTx	C_2H_5OH	40	1.41	0.80	0.61	0.76	3.38	1021
HMS−LTx	C_2H_5OH	50	0.95	0.90	0.05	0.06	3.06	1075
HMS−LTx	C_2H_5OH	60	0.93	0.88	0.05	0.06	2.50	1175
HMS−HTx	C_3H_7OH	20	1.74	0.76	0.98	1.29	2.70	1140
HMS−HTx	C_3H_7OH	30	1.28	0.72	0.56	0.78	2.66	1160
HMS−HTx	C_3H_7OH	40	0.75	0.59	0.16	0.27	2.15	1300
HMS−LTx	C_3H_7OH	50	0.62	0.60	0.02	0.03	2.10	1179
Al-HMS−HTx	C_2H_5OH	40	1.17	0.80	0.37	0.46	3.4	900
Al-HMS−LTx	C_2H_5OH	50	0.90	0.80	0.10	0.12	3.3	980
Al-MCM-41			0.95	0.85	0.10	0.11	3.3	1036

[a] All HMS materials were prepared at surfactant concentration of 0.23 M DDA and $S°/I° = 0.27$ and calcined at 630 °C. [b] V_t, total pore volume obtained from the volume of N_2 adsorbed at 0.99 P/P_0. [c] V_f, framework pore volume obtained from the volume of N_2 adsorbed at 0.50 P/P_0. [d] V_{tx}, textural pore volume obtained from the difference ($V_t - V_f$).

Table 2. Alkylation of 2,4-Di-*tert*-butylphenol with Cinnamyl Alcohol in the Presence of Al-HMS and Al-MCM-41 Catalysts[a]

catalyst (2.0 mol % Al)	conversion (%)	selectivity (%)	flavan yield (%)
Al−HMS−HTx	56.5	74.2	41.4
Al−HMS−LTx	49.1	69.3	34.0
Al−MCM-41	47.2	71.8	33.9

[a] Reaction conditions: 60 °C, 6 h, 500 mg catalyst, 50 mL isooctane.

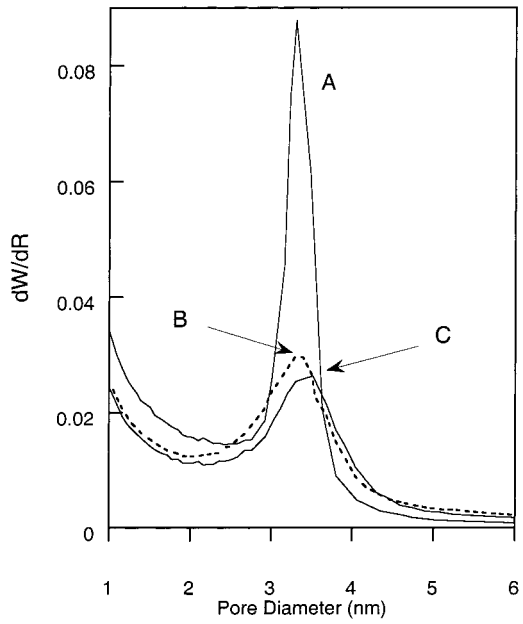

Figure 3. Horvath and Kawazoe pore-size distribution plot for calcined samples of 2% Al-substituted HMS and MCM-41 molecular sieves: (A) Al-MCM-41, (B) Al-HMS−LTx, and (C) Al-HMS−HTx. The average framework pore size is 3.35 ±0.05 nm for each sample.

as represented by the higher magnification TEM images (see Figure 4B and D, respectively).

Small angle scattering of both X-rays (SAXS) and neutrons (SANS) has been used quite extensively in probing the fractal dimensions, particles sizes and various other structural parameters of porous silicas[28,29] and micelles confined in porous

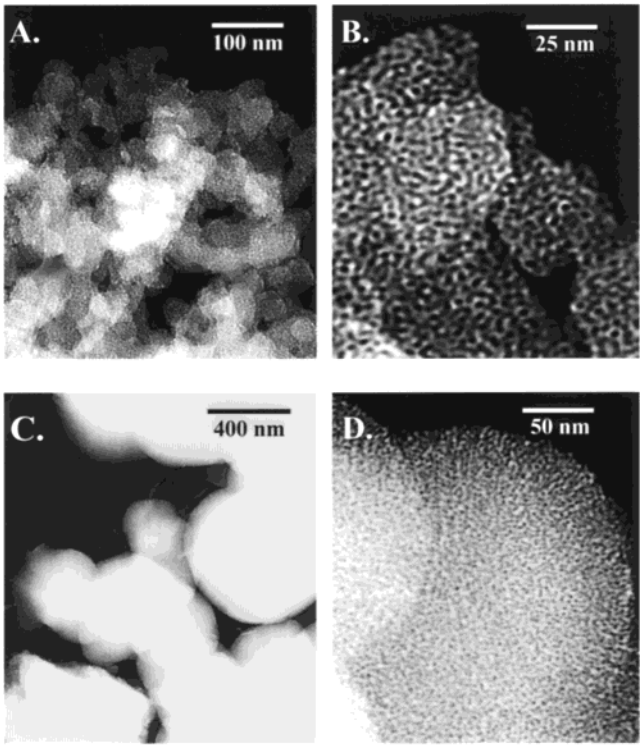

Figure 4. TEM images of calcined HMS materials assembled from heterogeneous emulsion [HMS−HTx, (A) Low magnification, (B) high magnification] and homogeneous solution [HMS−LTx, (C) Low magnification, (D) high magnification) forms of a dodecylamine surfactant in cosolvents containing 40 and 50% ethanol by volume, respectively.

silica.[30] In addition, several small-angle scattering studies have been reported for surfactant assembled mesostructured silicas.[31−35] SAXS also has recently been used to describe the unique mass

(28) Brinker, C. J.; Scherer, G. W. *Sol-Gel Science*; Academic Press: New York, 1990; p 184.

(29) Beelen, T. P. M.; Dokter, W. H.; van Gardren, H. F.; van Santen, R. A.; Pantos, E. *Preparation of Catalysts, VI*; Elsevier Science: New York, 1995, p 33.

(30) Bradley, K. F.; Chen, S.-H.; Thiyagarajan, P. *Phys. Rev. A.* **1990**, *42*(10), 6015.

(31) Auvray, L.; Ayral, A.; Dabadie, T.; Cot, L.; Guizard, C.; Ramsey, J. D. F. *Faraday Discuss.* **1995**, *101*, 235.

(32) Edler, K. J.; Reynolds, P. A.; White, J. W.; Cookson, D. *J. Chem. Soc., Faraday Trans.* **1997**, *93*(1), 199.

(33) Edler, K. J.; Reynolds, P. A.; White, J. W. *J. Phys. Chem. B* **1998**, *102*, 3576.

fractal character of surfactant-templated silica aerogels (STSA)[36] with a hexagonal MCM-41 framework structure (see below). To obtain more incisive insights into the texture of wormhole HMS−HTx and -LTx derivatives in comparison to hexagonal mesostructures, we examined the SAXS scattering over a wide q-range, $0.0003 < q < 0.7$ Å^{-1}. Over this q-range, we can attempt to determine the surface and mass fractal dimensions of the small particle materials by analyzing the transition region between surface and mass fractal power law scattering.

Small-angle scattering provides a direct measure of the fractal nature of matter[37] over many decades in length scale, $1/q$. This inverse relationship means that scattering by small feature sizes is observed at large q values and conversely, large feature sizes are probed at small q values. For example, the smallest features giving small-angle scattering intensity in the present case are the framework pores, whereas the large features contributing to the scattering are the porous particles themselves.

Fractal objects produce power law scattering, $I(q) = Cq^P$, where C is a constant and P is the power.[28] SAXS data are plotted as Intensity vs q on log−log scales such that power law scattering is seen as straight-line segments. Objects that scatter as $P = -4$ (Porod scattering) have a nonfractal surface morphology. Power laws where $-4 \leq P \leq -3$ are indicative of surface fractal structure where the surface fractal dimension $D_s = 6 + P$. The surface area of a surface fractal scales as $A \approx r^{D_s}$, where r is the size of the particle. Power laws where $-3 \leq P \leq -1$ are indicative of mass fractal structure where the mass fractal dimension $D_m = -P$. Mass fractals are porous aggregates of primary particles for which the mass scales as $M \approx r^{D_m}$. Power laws where $P < -4$ are indicative of diffuse interfaces.[38]

We first consider the small angle scattering characteristics of hexagonal mesostructured silicas formed through general electrostatic assembly pathways, in particular MCM-41[20,21,39] and SBA-3.[3] SAXS data, along with a least-squares fit to the power-law, are plotted in Figure 5. The curve for MCM-41 has been offset by a factor of 10^2 across the entire q range for clarity. Power-law scattering is seen in the low-q region with no evidence of a surface to mass fractal scattering transition. Multiple orders of correlation peaks are evident at high-q in both samples. A least-squares fit to the power-law scattering at mid-q (q lower than the correlation peaks) yields an exponent of −3.78(3) for SBA-3 and −3.62(2) for MCM-41, where the numbers in brackets are the standard deviation on the last figure. This implies that the surfaces of the primary particles are fractal with moderate roughness and a surface fractal dimension of 2.22 for SBA-3 and 2.38 for MCM-41(see Table 3).

The multiple correlation peaks evident in the scattering curves of MCM-41 and SBA-3 indicate that the pores are well ordered. Both curves are consistent with the hexagonal array of framework pores seen in TEM images. MCM-41 is the best-ordered structure with four correlation peaks and a d_{100} peak at 3.55 nm. Three correlation peaks are evident in SBA-3 with a d_{100} peak 3.51 nm.

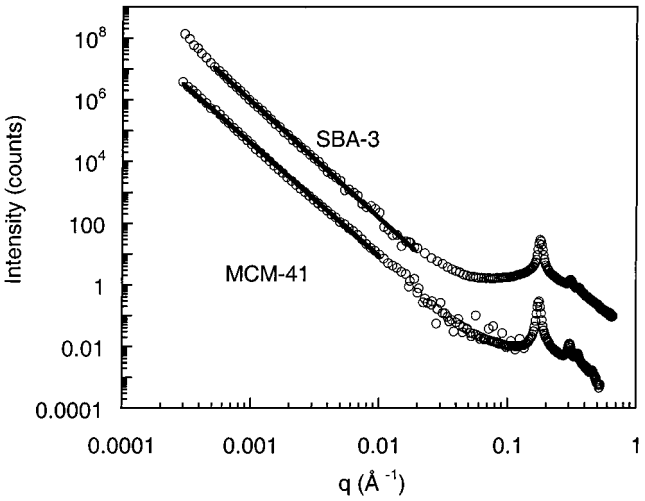

Figure 5. SAXS data for the hexagonal molecular sieve silicas SBA-3 and MCM-41 plotted as $I(q)$ vs q on log−log scales. The curve for MCM-41 has been offset by a factor of 10^2 counts across the entire range for clarity. The solid lines are fits to a power law equation, $I(q) \approx q^P$.

Table 3. Summary of SAXS Parameters for Mesostructured Molecular Sieves[a]

	HMS−HTx	HMS−LTx	SBA-3	MCM-41	STSA[b]
D_s	2.76	<2.00	2.22	2.35	2.0
D_m	1.83	2.87	NA	NA	1.0

[a] $D_s = 6 + P$, where P is the power-law slope of the mid-q (surface scattering) region. $D_m = -P$, where P is the power-law slope of the low-q region. [b] Surfactant-templated silica aerogel.[39]

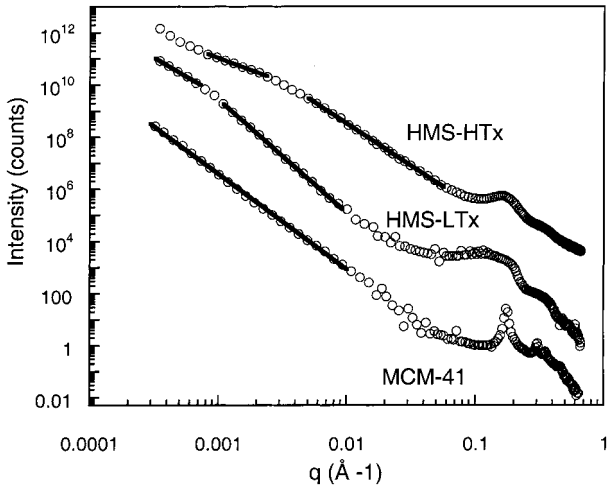

Figure 6. SAXS data for the molecular sieve silicas HMS−HTx, HMS−LTx, and MCM-41 plotted as $I(q)$ vs q on log−log scales. The curves have been offset from each other by a factor of 10^2 counts across the entire range for clarity. The solid lines are fits to a power law equation, $I(q) \approx q^P$.

The SAXS data, along with the least-squares fit to the power-law, for HMS materials are shown in Figure 6, along with the scattering curve of MCM-41 for comparison. Again, the curves are offset from each other by a factor of 10^2. The SAXS data for both HMS samples show a transition between two different power law scattering regimes. The mid-q power law is attributed to surface scattering from the primary particles, the low-q power law to scattering from mass fractal aggregates. The transition region occurs relative to the length scale of the primary particle. HMS−HTx displays a transition region at higher q than seen

(34) Aikawa, K.; Kaneko, K.; Fujitsu, M.; Tamura, T.; Ohbu, K. *Langmuir* **1998**, *14*, 3041.
(35) McGrath, K. M.; Dabbs, D. M.; Yao, N.; Aksay, A.; Gruner, S. M. *Science* **1997**, *277*, 552.
(36) Rieker, T. P.; Anderson, M. T.; Sawyer, P. S.; Rane, S.; Beaucage, G. In *Materials Research Society Symposium Proceedings*; Materials Research Society: San Francisco, CA, 1998; pp 95−99.
(37) Pfeifer, P.; Avnir, D. *J. Chem. Phys.* **1983**, *79*, 3558.
(38) Schmidt, P. W. *J. Appl. Crystallogr.* **1992**, *15*, 567 and references therein.
(39) Anderson, M. T.; Sawyer, P. S.; Rieker, T. *Microporous Mesoporous Mater.* **1998**, *20*, 53.

in HMS−LTx, indicating significantly smaller primary particle sizes.

HMS−HTx has a $D_s = 2.76$ over about a decade of q, the highest surface fractal dimension of any of the samples studied. It was also possible to estimate the mass fractal dimension of the particle aggregate from the power-law scattering on the low-q side of the crossover ($D_m = 1.83$). This latter value should be treated with some caution because the fit is over less than one decade of data. However, it is consistent with the clustering (intergrowth) of small mesostructured primary particles into larger textured aggregates, as observed in the TEM images. In addition, this SAXS result supports the conclusion that the higher catalytic activity of a HMS−HTx compared to that of a HMS−LTx analogue is primarily a consequence of improved molecular access to the pores of the wormhole framework.

The SAXS curve for HMS−LTx exhibits power-law scattering with a slope of −4.39. Such a steep slope of the power-law scattering has previously been seen in semicrystalline polymer samples that have a graded electron density at the surface due to a crossover between crystalline and amorphous regions.[38] This behavior also was observed for a separate HMS sample with a smooth spherical surface, as judged by TEM. A linear fit to the low-q side of the crossover point yielded $D_m = 2.87$. This is a mass fractal that is approaching the value of $D_m = 3.00$, as expected for a three-dimensional object. Again, the fit to the scattering data is over less than a decade of q. These SAXS data, however, are consistent with the TEM images showing continuous (monolithic) three-dimensional particles. Thus, we can conclude that HMS−LTx is composed of larger primary particles with a surface fractal dimension that is lower than HMS−HTx, but a higher mass fractal dimension. These factors contribute to a material with considerably less textural porosity than HMS−HTx, though the primary particles in either case are not as large as those found in either MCM-41 or SBA-3.

The significant textural porosity of HMS−HTx materials arises from a combination of the high surface texture and low mass fractal dimension of the porous silica aggregates. The hexagonally ordered materials prepared via electrostatic assembly pathways possessed particles larger than can be determined by the SAXS instrumentation used. Even though each of these materials does possess a moderate surface roughness, the lack of textural pore volume can be attributed to the large monolithic particles. Similarly, the smooth particle nature of the HMS−LTx material, combined with the nonfractal aggregation of the primary particles explains the lack of textural pore volume in this material.

Recent small angle scattering studies have shown that MCM-41 silicas synthesized through a modified aerogel technique[39] retain not only a high degree of framework pore order, but also form a low dimensional mass fractal monolith.[36] These surfactant-templated silica aerogels (STSA) upon supercritical solvent extraction and subsequent calcination, retain significant textural pore volume due to the low mass fractal dimension ($D_m = 1.0$) of the materials. Although the primary particles of STSA can be larger than those of HMS−LTx and the surfaces smooth ($D_s = 2.0$), their growth into a low dimension mass fractal ($D_m = 1$ vs $= 2.87$) results in significant interparticle porosity (Table 3).

The analysis of the high-q (small feature size) region of the SAXS gives information about the framework pore sizes and separations. The HMS samples show only a single, broad correlation peak and no higher order reflections, in accord with the wide-angle XRD results. The presence of only one correlation peak indicates that a pore-pore correlation exists due to the more or less uniform pore diameter and wall thickness, but that the pores are not arranged in a periodic array. An additional feature is evident in the data on the high-q side of the correlation peaks in both HMS samples, but it cannot be indexed as a higher order reflection. We believe that this small angle scattering feature arises from the wormlike framework pores. A quantitative analysis is in progress and will be reported elsewhere.

Conclusions

The textural properties of HMS molecular sieves with wormhole framework structures are determined by the physical state of the neutral amine surfactant used to direct the S°I° assembly process. Homogeneous solutions of the structure-directing surfactant in water:alcohol cosolvents containing relatively high volume fractions of alcohol (i.e., ≥70% methanol, ≥50% ethanol, or ≥50% propanol) completely dissolve the surfactant and allow for the formation of HMS−LTx derivatives with low textural pore volumes (<0.1 cm^3/g). The uniform nucleation and growth of HMS−LTx derivatives from these homogeneous surfactant solutions results in monolithic particles with smooth surfaces, as judged by TEM and SAXS. The textural properties of HMS−LTx derivatives are similar to those of hexagonal MCM-41 and SBA-3 mesostructures assembled through electrostatic assembly pathways.

Increasingly polar cosolvent compositions partition the surfactant between homogeneous solution and emulsion forms. These heterogeneous mixtures of the surfactant afford HMS−HTx derivatives in which the textural mesoporosity can be as high as 1.1 cm^3/g without compromising the framework pore volume or framework pore size. The strong correlation between high textural mesoporosity and surfactant heterogeneity suggests that primary HMS particles are not nucleated from the homogeneous solution phase of the surfactant mixture but that they form and intergrow at the surface of colloidal particles of the free surfactant in emulsion form. As the primary particles undergo further intergrowth and deplete the emulsion, voids reminiscent of the segregated surfactant form within the aggregates and give rise to the high textural mesoporosity. That the primary particles grow nonuniformly is supported by the high surface fractal dimension ($D_s = 2.7$) and low mass fractal dimension ($D_m = 1.83$) obtained from the SAXS studies.

Finally, the results of the present study clearly show that the catalytic activity of a HMS molecular sieve for a sterically demanding condensed phase reaction, such as the alkylation of 2,4-di-*tert*-butylphenol with cinnamyl alcohol, is greatly dependent on the textural mesoporosity available for transporting reagents to the framework mesopores. An Al-HMS−HTx derivative affords up to 1.20 times more alkylation product than either Al-HMS−LTx or MCM-41 with the same aluminum content and framework pore size. The assembly of a catalytically superior HMS−HTx derivative, as opposed to a less active HMS−LTx form, is very sensitive to the alcohol content of the cosolvent. A change in alcohol content as low as 10 vol % can decide the difference in textural mesoporosity and catalytic performance properties. Previously reported discrepancies in the catalytic activities of HMS molecular sieves, in comparison to MCM-41.[17,18] most likely were a consequence of differences in the cosolvent dependent textural mesoporosities. Thus, care must be exercised in selecting the alcohol composition of the cosolvent during the synthesis of a HMS molecular sieve catalyst with high textural porosity and catalytic activity. The catalytic

importance of textural mesoporosity can also be anticipated for electrostatically ordered mesostructures, such as the STSA[36] forms of MCM-41.

Acknowledgment. The support of this research through NSF CRG Grants CHE-9633798 and -9903706 is gratefully acknowledged. Y.L. acknowledges support from the K.C. Wong Foundation. S.J.L.B. acknowledges support from the Alfred P. Sloan Foundation, and T.P.R. acknowledges financial support from Sandia National Laboratories, which is operated for the U.S. Department of Energy under contract number DEAC04-99AL85000.

JA991400T